NANO LETTERS

2008
Vol. 8, No. 12
4128-4133

Förster-Type Resonant Energy Transfer Influenced by Metal Nanoparticles

Frank Reil,* Ulrich Hohenester, Joachim R. Krenn, and Alfred Leitner

Karl-Franzens Universität Graz, Institut für Physik, Universitätsplatz 5, 8010 Graz, Austria

Received May 23, 2008; Revised Manuscript Received September 12, 2008

ABSTRACT

We show experimentally and numerically that Förster-type resonant energy transfer between molecules strongly depends on the interaction with plasmonic resonances in a nearby metallic nanoparticle (MNP). Acceptor luminescence emerges at the expense of donor luminescence when an acceptor molecule harvests the donor's near-field energy. By tuning the resonance of a close-by MNP across the transition energy bands of the molecules, we show how the molecular luminescence is affected and in part even strongly increased.

Over the past years, the interaction of fluorescing dye molecules with plasmons in metallic nanostructures has gained increasing interest.[1−7] Metallic nanoparticles (MNPs) which support particle plasmons oscillating in the visible or infrared region are the main focus of research due to their ability to influence electronic transitions of a luminescent molecule in the absorption and the emission channel. In the latter, both radiative and nonradiative rates are generally affected due to a change in the optical local density of states (LDOS) induced by the MNP.[8,9] In other terms, the nanoantenna efficiency of the fluorophore−MNP system is modified and additional damping is introduced by the MNP. The degree of change depends on the spectral overlap of the molecule's absorption and luminescence bands with the plasmonic resonance of the MNP but also on the position and orientation of the molecule relative to the MNP.[10]

Even for strong MNP-mediated radiative decay rate enhancements, the emitted "steady-state" light intensity can decrease, namely, when the ratio of radiative to nonradiative rates decreases due to Ohmic losses in the MNP.[11] This is generally the case for molecules with a high intrinsic emissive quantum yield, i.e., with intrinsically small nonradiative rates, where Ohmic losses introduced by the MNP have a major effect on the aforementioned ratio.[5] Nevertheless, the enhancement by plasmonic nanoantennas of emitters with even a high quantum yield has been observed.[10]

MNPs are also capable of influencing the resonant near-field energy transfer between two close molecules, known as Förster resonance energy transfer (FRET). Here, a donor-fluorophore excites a close-by acceptor-fluorophore through its near-field, when the corresponding emission and excitation bands of donor and acceptor overlap sufficiently.

The first theoretical modeling of FRET in interaction with metal nanoparticles by Gersten and Nitzan[12] in the early 80s predicted an enhancement of the transfer rate up to 6 orders of magnitude when introducing a MNP between a donor and an acceptor for sufficiently large donor−acceptor separations. Another study[13] showed the enhancement of the donor emission for a donor−acceptor layer when applied to a nanogranular metal ("silver-island") film. Later, Andrew and Barnes[14] experimentally verified the theoretical predictions[12] of enhanced energy transfer from a donor to an acceptor layer separated by a flat metal sheet. Lakowicz and co-workers[15] investigated FRET pairs connected to opposite ends of double helical DNA, yielding a donor−acceptor separation at which the Förster transfer efficiency is weak. Introducing such molecules to nanoscopic silver particles resulted in a dramatic increase in FRET.

Systems comprised of FRET pairs and MNPs show a rich variety of behaviors. Many physical processes involved remain unclear; a major experimental shortcoming in past studies has been the inavailability of MNPs with uniform plasmonic resonances placed at well-defined positions with respect to the FRET pairs. But, in order to understand the physics behind MNP-modified FRET, wavelength and spatially resolved investigations of the interactions between donor, acceptor, and MNP are necessary. Today's electron-beam lithography enables the fabrication of MNP arrays with well-defined and uniform resonances. In the present paper we experimentally and theoretically investigate the influence of MNP arrays with various resonance wavelengths on the FRET process by observing the changes in the emission spectra of both donor and acceptor.

Förster-type resonant energy transfer occurs between an excited donor and an acceptor molecule when their emission and absorption bands overlap sufficiently and their mutual distance is not much larger than the Förster radius R_F. The latter is defined as the distance of a pair of donor and acceptor

10.1021/nl801480m CCC: $40.75
Published on Web 10/29/2008

at which the FRET efficiency is 50%. Its precise value depends on the details of the donor−acceptor complex, such as dipole orientation factor and the spectral overlap between donor emission and acceptor absorption, and is typically about 5 nm. The FRET efficiency, which depends on the radiative and molecular decay rates $\gamma_{r,D}^0$ and $\gamma_{m,D}^0$ of the donor in the absence of the acceptor and the FRET rate $\gamma_{FRET}^0 = \gamma_D^0(R_F/R)^6$ at a given donor−acceptor distance R, can be expressed as

$$E_{FRET}^0(R) = \frac{\gamma_{FRET}^0(R)}{\gamma_D^0 + \gamma_{FRET}^0(R)} = \frac{R_F^6}{R^6 + R_F^6} \quad (1)$$

where $\gamma_D^0 = \gamma_{r,D}^0 + \gamma_{m,D}^0$ is the sum of radiative and molecular decay rates. In the following we consider the situation where a uniform distribution of donor and acceptor molecules with concentrations n_D and n_A is placed on a planar substrate. If n_A is sufficiently low, such that the probability for a donor molecule interacting with two or more acceptors is small, the FRET probability is obtained by summing over all transfer processes according to

$$P_{FRET}^0 \approx n_A 2\pi \int_0^\infty E_{FRET}^0(R) r\, dr = \frac{2\pi^2}{3\sqrt{3}} n_A R_F^2 \approx 1.21 \frac{n_A}{n_0} \quad (2)$$

with $n_0 = 1/(\pi R_F^2)$ being the *critical* density. Equation 2 is inappropriate for higher acceptor concentrations, where one donor molecule can interact with several acceptor molecules, as is the case in our experiments. Thus we first compute the average decay of a single donor molecule

$$I_D^0(t) = \exp\left[-\gamma_D^0\left(t + 1.354\frac{n_A}{n_0}t^{1/3}\right)\right] \quad (3)$$

where the first term in the exponential describes the radiative and molecular decay and the second one the decay associated with the Förster transfer. The $t^{1/3}$ dependence of the population decay is due to the two-dimensional geometry of the donor−acceptor complex and differs from the usual $t^{1/2}$ dependence for a three-dimensional geometry.[17−19] The FRET probability is then obtained from eq 3 according to $P_{FRET}^0 = 1 - \gamma_D^0 \int_0^\infty I_D^0(t)\, dt$. Under continuous wave excitation conditions the donor molecules become populated with probability p_D, and the integrated donor and acceptor fluorescence intensities are

$$I_D^0 = p_D n_D (1 - P_{FRET}^0) q_D^0$$
$$I_A^0 = p_D n_D P_{FRET}^0 q_A^0 \quad (4)$$

with $q_D^0 = \gamma_{r,D}^0/\gamma_D^0$ and $q_A^0 = \gamma_{r,A}^0/\gamma_A^0$ being the quantum yield for the donor and acceptor, respectively.

(The decay of a single donor molecule interacting with several acceptors is of the form[16,17]

$$I_D^0(t) = \left\langle \exp\left(-\gamma_D^0\left[1 + \sum_\nu \left(\frac{R_F}{R_\nu}\right)^6\right]t\right)\right\rangle$$

with R_ν denoting the different acceptor positions and the brackets indicating a suitable ensemble average. Denoting by P_ν the probability that an acceptor is located at R_ν, we can write the ensemble average as[16]

$$I_D^0(t) = e^{-\gamma_D^0 t} \prod_\nu \left(1 - P_\nu + P_\nu e^{-\gamma_D^0 t (R_F/R_\nu)^6}\right) \cong e^{-\gamma_D^0 t} \exp\left[-\sum_\nu P_\nu \left(1 - e^{\gamma_D^0 t (R_F/R_\nu)^6}\right)\right]$$

where we have assumed $P_\nu \ll 1$ in order to arrive at the last expression. Converting the sum over acceptor positions into an integral over R, we obtain[18]

$$I_D^0(t) = e^{-\gamma_D^0 t} \exp\left[-2\pi n_A \int_{R_{min}}^\infty (1 - e^{-\gamma_D^0 t (R_F/R)^6}) R\, dR\right]$$

with R_{min} being a cutoff associated with the maximum transfer rate. Performing the integration in the above expression we then get eq 3, where the constant is given by $-1/3\Gamma(-1/3)$.)

The presence of a MNP modifies the decay rates of donor and acceptor. The electromagnetic field, in particular the near-field of a donor molecule, can drive a plasmonic oscillation of a nearby MNP, which leads to an enhancement of the radiative decay rate γ_r but also to Ohmic losses which increase γ_{abs}.[1,11,20] In addition, in the presence of the MNP the Förster energy resonance transfer rate $\gamma_{FRET} = \eta\gamma_{FRET}^0$ becomes enhanced by a factor $\eta(R)$.[21,22] The enhancement of the different rates has two major effects. First, the FRET efficiency

$$E_{FRET}(R) = \frac{\gamma_{FRET}(R)}{\gamma_D + \gamma_{FRET}(R)} \quad (5)$$

changes. Depending on the relative strength of the FRET enhancement $\eta(R)$ and the donor decay rate $\gamma_D = \gamma_{r,D} + \gamma_{abs,D} + \gamma_{m,D}^0$, this will lead to either an increase or decrease of the effective Förster radius and the FRET efficiency. Second, the quantum yields of the donor and acceptor become modified according to

$$q_D = \frac{\gamma_{r,D}}{\gamma_{r,D} + \gamma_{abs,D} + \gamma_{m,D}^0}$$
$$q_A = \frac{\gamma_{r,A}}{\gamma_{r,A} + \gamma_{abs,A} + \gamma_{m,A}^0} \quad (6)$$

which results in either an enhancement or reduction with respect to the free-molecule values. Which of these effects dominates depends critically on the properties of the donor−acceptor complex and the MNP.

We chose a europium^{3+} complex (tris(dibenzoylmethane)mono(1,10-phenanthroline)europium(III), in the following called "EuIII") as the donor and Cy5 dye (1,1′,3,3,3′,3′-hexamethylindodicarbocyanine iodide) as the acceptor molecule. EuIII emits a narrow line at 612 nm when excited by light at 360 ± 20 nm. Cy5 absorbs in a broad band mainly between 580 and 680 nm and emits also broadly between 650 and 700 nm. The Förster radius for this FRET pair is calculated to be 5.6 nm.[23] The donor and acceptor molecules were deposited onto the sample by direct vacuum sublimation.

Luminescence spectra are obtained with a Zeiss Axioscope microscope fluorimeter in epiconfiguration equipped with a spectrograph (Jobin Yvon UFS200) and detected by a single-photon sensitive camera (DV885 LC-VT by Andor). The excitation source is a mercury lamp filtered with appropriate band-pass filters of 365 nm and fwhm of 20 nm. Its light is focused onto the sample by a microscope objective (Zeiss

Achroplan, 20×, NA = 0.5), resulting in a spot of approximately 150 μm diameter with an intensity of about 5.8 W/cm ^{2}. The luminescence light is filtered by an edge filter Zeiss LP595 which cuts off wavelengths below 600 nm.

The resulting molecular surface density on the bare sample (without MNPs) was determined by measurements of the fluorophores' characteristic absorbance spectra in the blue curve of Figure 1 a. According to the Lambert−Beer law

$$\mathrm{Abs} = dc_V\epsilon \tag{7}$$

where Abs is the measured absorbance, d the length of the sample in centimeters, and c_V the molar volume concentration in mol/L. ϵ is the dye-specific molar extinction coefficient; it is 2.5×10^5 L/(mol cm) for Cy5 and 6×10^4 L/(mol cm) for EuIII. Assuming that the absorption cross section does not differ considerably in solution and on the substrate, we obtain for the molar surface density c_A in mol/cm^2

$$c_A = \frac{\mathrm{Abs}}{10^3\epsilon} \tag{8}$$

We get 4.29 molecules/nm^2 EuIII and 0.16 molecules/nm^2 Cy5 which amounts to a EuIII:Cy5 ratio of approximately 26:1. This high concentration of EuIII is necessary due to its comparably small emission output as a result of its small molar extinction coefficient.

The MNP arrays are prepared by means of an electron-beam lithography technique. The disk-shaped particles are arranged as a quadratic lattice with a pitch of 100 nm on top of a borosilicate glass substrate with a thin indium tin oxide (ITO) layer for charge removal during the lithography process and a 10 nm SiO_2 layer, which prevents the dye molecules between the MNPs from quenching. A second 10 nm thick SiO_2 layer is applied on top of the array; it creates a distance between fluorophores and MNPs to minimize quenching and to provide a uniform surface for the dye molecules. In addition, its rough surface prevents dye molecules from wandering across the surface, which would lead to inhomogeneities in their surface density.

Figure 1b illustrates the makeup of such an MNP array covered with dye molecules. The particles have a height of approximately 15 nm and diameters of 30−80 nm. Beginning at 30 nm, those diameters were gradually increased in the electron lithographic process, resulting in narrowly spaced plasmonic resonances covering a range from about 560 to 680 nm (see top axis of Figure 3). The plasmon resonances were determined by far-field measurements of the absorption, using a microscope spectrometer in transmission equipped with a Zeiss Achroplan 10×, NA = 0.25 objective. The blue curve in Figure 1a shows the absorbance spectrum curve of an array of 55 nm disks, centered at a wavelength of 622 nm.

Figure 2 compares the luminescence spectra of three different molecular surface layers irradiated under identical conditions at around 365 nm. The blue curve representing a pure EuIII donor layer on the substrate (4.29 molecules/nm^2) shows an intensity maximum of 1.35×10^5 counts at 610 nm (note the multiplication by $^1/_{50}$ to fit the scale). The red curve represents the luminescence from the same donor concentration, but with acceptors added at a density of 0.24 molecules/nm^2. Here, the donor intensity is 500-fold reduced

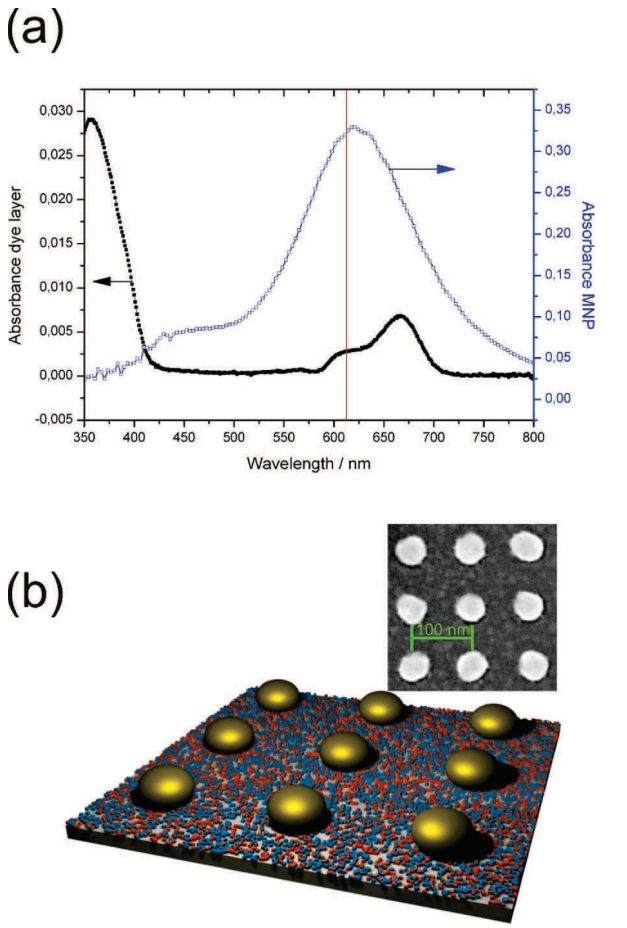

Figure 1. (a) Black curve: Absorbance of coevaporated mixture of 4.29 molecules/nm^2 EuIII and 0.16 molecules/nm^2 Cy5. The narrow absorption peak at about 360 nm belongs to EuIII, the broad peak between 600 and 700 nm to Cy5. Red line: Emission line of EuIII at 612 nm. Blue curve: Absorbance of typical MNP, here centered at 622 nm. (b) Bottom left: Schematic drawing of nanodisk array with donor and acceptor molecules placed in between. The molecules on top of the particles are not shown. Top right: SEM picture of a typical MNP array with a 10 nm thick SiO_2 layer on top.

to 270 counts, whereas a strong and broad acceptor peak appears, demonstrating the presence of a strong Förster transfer. Thus, by the action of FRET the effective quantum efficiency of the donor is reduced from 0.4 to 0.005. We can calculate the acceptor's quantum efficiency by comparing the numbers of emission quanta of the pure EuIII-layer with that of the emerging Cy5 in the mixed layer, which is performed by numerical integration over the respective spectral peaks. Another requirement for the validity of this calculation is that the acceptor is exclusively and strongly excited by the donor and not the 365 nm pump light we employ. This was verified experimentally with a pure Cy5-layer. Using the data of Figure 2, we obtain an averaged acceptor quantum efficiency of 0.005. Finally, the black curve shows the same dye layer on top of an MNP array with particle plasmon resonances at 625 nm, which is slightly red-shifted with respect to the donor's emission at 612 nm. We find a strong regrowth of the donor's luminescence from 270 counts to 1900 counts, yielding an emission enhancement factor of 7 and a weaker acceptor emission enhancement of

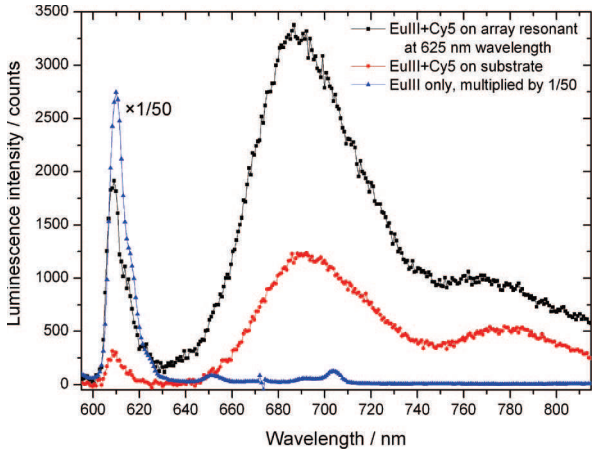

Figure 2. Luminescence intensity of 4.29 molecules/nm^2 EuIII and 0.28 molecules/nm^2 Cy5 on top of an MNP array with a resonance wavelength of 625 nm (black squares) and the bare substrate next to the array (red circles). Also shown is the EuIII luminescence spectrum with the same amount of EuIII but without Cy5 (blue triangles), multiplied by a factor $^1/_{50}$.

about a factor 2.7. Other mechanisms for the observed luminescence enhancement in the presence of MNPs can be excluded: As already mentioned, the acceptor itself displays no significant fluorescence for an excitation wavelength around 365 nm. Also, the donor excitation enhancement by MNPs is no more than 40%, as our numerical calculations indicate. At this wavelength, gold shows a strong absorption. We are going to present details of this calculation in a future publication.

The enhancement factors (EFs) for arrays covering a range of wavelengths under the same experimental conditions are shown as filled symbols in Figure 3. The EF is defined as the ratio of luminescence intensity on top of a given MNP array to that on the bare glass−ITO−SiO_2 substrate; see above.

The EF for EuIII (blue filled triangles) shows a pronounced maximum at a wavelength red-shifted from the EuIII emission line at about 625 nm, while the EF of Cy5 (green filled circles) peaks at about 660 nm. At those wavelengths, the MNP-mediated quantum yield enhancement of the respective dyes becomes maximal. Other phenomena, such as the increasing radiative dipole moment at larger particle volumes and therefore wavelengths, are included in our numerical calculations and were shown to be not responsible for the observed wavelength dependence of the enhancement factors.

The open symbols in Figure 3 show the enhancement factors of the same FRET dye ensemble on the same MNP-array sample, but with just 0.20 molecules/nm^2 Cy5, which is about 30% less than before. The EF of EuIII (black open triangles) is less pronounced now, because its initial quantum efficiency is larger, leaving less room for enhancement. It reaches only a value of 3.0. The EF of Cy5 (red open circles) is also weaker than before; it peaks at 2.5.

To analyze the experimental results, we additionally performed numerical calculations based on the boundary element method (BEM).[24,25,11,20] We consider a cylinder-like

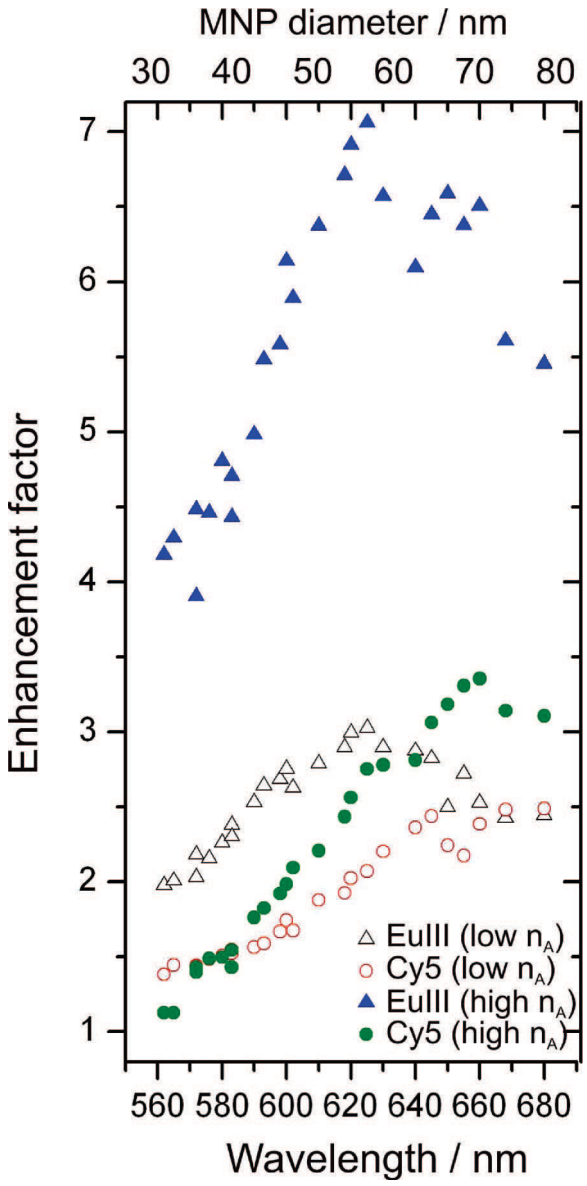

Figure 3. Luminescence enhancement factors (EFs) for EuIII and Cy5 on top of MNP arrays with resonance wavelengths ranging from 560 to 680 nm (bottom axis), corresponding to disk diameters of 30−80 nm (top axis). Open symbols ("low n_A"): EFs of EuIII (black triangles) and Cy5 (red circles) for concentrations of 4.29 molecules/nm^2 EuIII and 0.20 molecules/nm^2 Cy5. Filled symbols ("high n_A"): EFs of EuIII (blue triangles) and Cy5 (green circles) for concentrations of 4.29 molecules/nm^2 EuIII and 0.28 molecules/nm^2 Cy5.

gold nanoparticle with a diameter of 60 nm and a height of 15 nm and assume that donor and acceptor molecules are placed on a sheet enclosing the MNP, as depicted in Figure 4c. The area of the circular sheet approximately corresponds to the effective active area of one nanoparticle in the square arrangement of the experiments. The distance between the molecular sheet and the MNP is set to 10 nm. The emission spectra of the donor (acceptor) are assumed to be Gaussian with a center wavelength of 615 nm (675 nm) and a full width at half-maximum of 15 nm (35 nm). The acceptor's absorption spectrum is assumed to be constant within the donor emission band. Quantum yields of donor and acceptor are set to $q_D{}^0 = 0.4$ and $q_A{}^0 = 0.005$, respectively, which

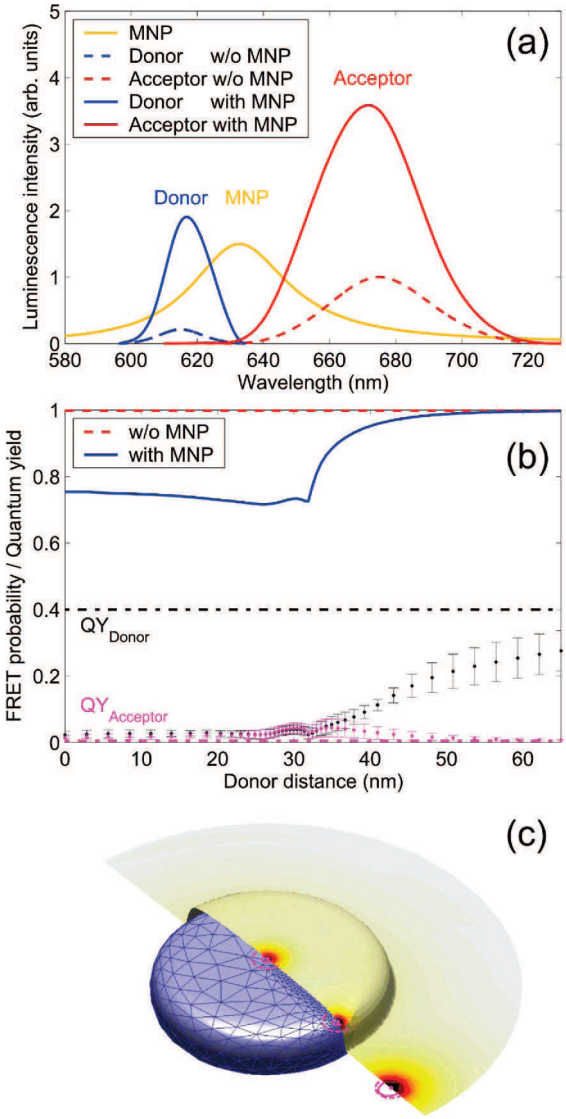

Figure 4. Results of our numerical calculations. (a) Fluorescence spectra with (solid lines) and without (dashed lines) the metallic nanoparticle. The bright, orange line indicates the scattered intensity of the metallic nanoparticle in absence of donor and acceptor molecules. (b) FRET probability in the presence (solid line) and absence (dashed line) of the metallic nanoparticle, as a function of the distance from the center of the MNP (see panel c). The symbols and dotted lines in the lower part of the panel show the quantum yield QY for the donor and acceptor in the presence and absence of the MNP. The error bars indicate the spread of the transition energies of donor and acceptor around their respective center values. (c) Surface discretization of cylinder-shaped particle (60 nm diameter and 15 nm height) as used in our BEM calculations. The donor and acceptor molecules are placed on a sheet with a distance 2 nm away from the MNP. The color map shows the FRET probability for three selected donor positions. The solid and dashed lines indicate the effective Förster radii for the donor−acceptor complex in the presence and absence of the MNP.

results in a reduction of the donor luminescence by a factor of approximately 700 in the presence of the acceptors. We calculate the enhancement of the radiative and nonradiative decay rates from the imaginary part of Maxwell's Green function,[1,20] which is computed in the quasi-static limit and for the gold dielectric function of ref 26. Coupling effects between the MNPs can be neglected due to their large mutual distances of 100 nm, as our numerical calculations indicate. The enhancement of the Förster rate is calculated from the square modulus of the Green function, for given donor and acceptor positions,[21] and the fluorescence spectra are finally obtained by averaging over all donor and acceptor positions. In our calculations we assume that the orientations of the donor and acceptor dipoles are randomly distributed. There is indeed a strong dependence of the interaction between dye molecules and MNPs on the molecule's orientations, which will be the subject of a future publication.

Figure 4a shows the luminescence spectra in absence (dashed lines) and presence (solid lines) of the MNP, along with the scattered intensity of the nanoparticle whose center frequency is located in between the donor and acceptor fluorescence peaks. One observes that in the presence of the MNP the donor and acceptor fluorescences become enhanced by factors of 8.6 and 3.5, respectively. As is apparent from panel b, the enhancement of the donor fluorescence is due to a dramatic break-in of the FRET probability. A more detailed analysis reveals that P_{FRET} drops as a result of the strong enhancement of the radiative and nonradiative donor decay rates, whereas the enhancement of the Förster transfer has no significant impact on the fluorescence properties. The reason why the enhancement of the donor emission is not much larger is due to the strong decrease of the quantum yield q_{D} associated with Ohmic losses in the MNP. On the other hand, the small acceptor quantum yield becomes enhanced in the prescence of the MNP, resulting in an enhancement of the acceptor fluorescence despite the break-in of the Förster transfer. Additional calculations on disk-shaped MNPs with different plasmonic resonances qualitatively agree with the experimental data in Figure 3, but there are still certain quantitative discrepancies due to the changing rate-enhancing areas for FRET (compare)[15] and the various fluorophore decay rates, which we would like to resolve first before publishing.

In this work, we have shown that metallic nanoparticles can modify the Förster transfer between two molecules. By tuning the plasmonic resonance wavelength of an MNP close to the emission wavelengths of the donor, the MNP transforms part of the donor's near-field energy into light, at the expense of the Förster transfer rate and other nonradiative processes. In addition, the emission intensity of the acceptor is strongly enhanced, when the MNP's resonance wavelength approaches the acceptor's emission wavelength. Our experimental results are corroborated by our numerical calculations based on the boundary element method.

Acknowledgment. We gratefully acknowledge the financial support provided by the European Union, Project No. FP6 2002-IST-1-507879, and the Erwin Schrödinger Institute for Nanoscale Research.

References

(1) Anger, P.; Bharadwaj, P.; Novotny, L. *Phys. Rev. Lett.* **2006**, *96*, 113002.
(2) Dulkeith, E.; Ringler, M.; Klar, T. A.; Feldmann, J.; Munoz Javier, A.; Parak, W. J. *Nano Lett.* **2005**, *5*, 585.
(3) Fort, E.; Grésillon, S. *J. Phys. D: Appl. Phys.* **2008**, *41*, 013001.

(4) Kalkbrenner, T.; Håkanson, U.; Sandoghdar, V. *Nano Lett.* **2004**, *4*, 2309.
(5) Reil, F.; Gerber, S.; Krenn, J. R.; Leitner, A. *J. Opt. A: Pure Appl. Opt.* **2007**, *9*, 437.
(6) Tam, F.; Goodrich, G. P.; Johnson, B. R.; Halas, N. J. *Nano Lett.* **2007**, *7*, 496.
(7) Zhang, J.; Lakowicz, R. *Opt. Exp.* **2007**, *15*, 2598.
(8) Martin, O. J. F.; Girard, C.; Dereux, A. *Phys. Rev. Lett.* **1995**, *74*, 526.
(9) Barnes, W. L. *J. Mod. Opt.* **1998**, *45*, 661.
(10) Muskens, O. L.; Giannini, V.; Sánchez-Gil, J. A.; Gómez, J. *Nano Lett.* **2007**, *7*, 2871.
(11) Gerber, S.; Reil, F.; Hohenester, U.; Schlagenhaufen, T.; Krenn, J. R.; Leitner, A. *Phys. Rev. B* **2007**, *75*, 073404.
(12) Gersten, J.; Nitzan, A. *J. Chem. Phys.* **1981**, *75*, 785.
(13) Leitner, A.; Reinisch, H. *Chem. Phys. Lett.* **1988**, *146*, 349.
(14) Andrew, P.; Barnes, W. L. *Science* **2004**, *306*, 1002.
(15) Lakowicz, J. R.; Kuśba, J.; Shen, Y.; Malicka, J.; D'Auria, S.; Gryczynski, Z.; Gryczynski, I. *J. Fluoresc.* **2003**, *13* (1), 69.
(16) Huber, D. L. *Phys. Rev. B* **1985**, *31*, 6070.
(17) Förster, T. *Z. Naturforsch., A* **1949**, *4*, 321.
(18) Parkinson, P.; Aharon, E.; H Chang, M.; Dosche, C.; Frey, G. L.; Köhler, A.; Herz, L. M. *Phys. Rev. B* **2007**, *75*, 165206.
(19) Herz, L. M.; Silva, C.; Friend, R. H.; Phillips, R. T.; Setayesh, S.; Becker, S.; Marsitsky, D.; Müllen, K. *Phys. Rev. B* **2001**, *64*, 195203.
(20) Hohenester, U.; Trügler, A. *IEEE J. Sel. Top. Quantum Electron.* **2008**, arXiv:0801.3900.
(21) Trung Dung, Ho.; Knöll, L.; Welsch, D. G. *Phys. Rev. A* **2002**, *65*, 043813.
(22) Govorov, A. O.; Lee, J.; Kotov, N. A. *Phys. Rev. B* **2007**, *76*, 125308.
(23) Selvin, P. R.; Rana, T. M.; Hearst, J. E. *J. Am. Chem. Soc.* **1994**, *116*, 6029.
(24) Garcia de Abajo, F. J.; Howie, A. *Phys. Rev. B* **2002**, *65*, 115418.
(25) Hohenester, U.; Krenn, J. R. *Phys. Rev. B* **2005**, *72*, 195429.
(26) Johnson, P. B.; Christy, R. W. *Phys. Rev. B* **1972**, *6*, 4370.

NL801480M